ADVANCED FUNCTIONAL MATERIALS

Fabrication of a Highly Transparent Conductive Thin Film from Polypyrrole/Poly(methyl methacrylate) Core/Shell Nanospheres

By *Jyongsik Jang** and *Joon Hak Oh*

Polypyrrole (PPy)/poly(methyl methacrylate) (PMMA) core/shell nanospheres with diameters of several tens of nanometers have been synthesized by two-step microemulsion polymerization, and highly transparent conductive thin films have been fabricated using the nanospheres as a filler in a PMMA matrix. The PPy/PMMA core/shell nanoparticles and their composite films have been extensively characterized using transmission electron microscopy (TEM), scanning electron microscopy (SEM), energy-dispersive X-ray spectroscopy (EDX), differential scanning calorimetry (DSC), thermogravimetric analysis (TGA), Fourier-transform infrared (FT-IR) and UV-vis spectroscopies, and electrical-conductivity measurements. The fabricated polymer films containing the PPy/PMMA core/shell nanofillers show a much better transparent conductive performance than that of uncoated PPy nanoparticles with similar dimensions or bulk PPy particles with diameters of several hundreds of nanometers. The PMMA shell promotes compatibility of the conductive fillers with the PMMA matrix and enhances dispersion of the PPy/PMMA core/shell nanofillers. In addition, the nanometer-thick PMMA shell has a lower glass-transition temperature (T_g), and can be effectively annealed to form a conductive-filler network with a high electrical conductivity at a relatively low filler content.

1. Introduction

Over the last two decades there has been a significant increase in the development of transparent conductive thin films owing to their diverse important applications in current technologies such as electrochromic and liquid-crystal displays, photovoltaic cells, heat mirrors, and electromagnetic-interference shielding. To date, the preparation of transparent conductive thin films has been largely dependent upon inorganic and metallic materials,[1] whereas relatively less attention has been paid to the application of organic materials.

In general, conducting polymers themselves possess poor mechanical properties, for example, brittleness and poor processability. These drawbacks can be overcome, however, by forming blends or composites with other polymer matrices with good tractability.[2] Although many different conducting polymer composites have been developed, their application to transparent conductive materials has rarely been investigated. In most cases, optically transparent conductive polymer films have been prepared by casting a solution containing soluble conducting polymers.[3] This method, however, needs additional chemical modifications to endow an infusible conducting polymer with solubility. In addition, the coating thickness should be very thin in order to remain highly transparent.

Huijs and co-workers have prepared transparent polymer films with an electrical conductivity in the antistatic range using polypyrrole (PPy)-coated latex particles with a diameter of about 700 nm.[4] These composite films show a sharp percolation threshold at around 0.25 wt.-% PPy content. However, the transparency deteriorates rapidly with increasing conductive-filler content, and the conductivity is reduced significantly by heat treatment. The reason for this is thought to be related to the size of the conductive composite filler and large-scale aggregation owing to poor compatibility with the matrix.

To obtain a highly transparent film, conductive powders should have an average particle diameter (approximately 0.2 μm), no greater than half of the shortest wavelength of visible light,[5] and ultrathin networks of conductive fillers should be formed in the transparent matrix.[6] It is quite difficult in the synthesis of polymer nanoparticles to reduce the particle size due to the thermodynamically and kinetically unstable polymerization conditions and particle–particle aggregation.

Recently, we have successfully synthesized conducting-polymer nanoparticles with diameters of several nanometers by low-temperature microemulsion polymerization.[7] Microemulsion micelles could be utilized as "nanoreactors" for the synthesis of PPy nanoparticles. They could also play an important role in determining the spherical morphology of the final product. In addition, the crosslinked characteristic of PPy chains, resulting from an α–β coupling reaction, endows the polymer nanoparticles with mechanical robustness. Considering the feasibility that a highly transparent performance might be obtained if these conductive organic particles were effectively dispersed in a transparent medium, we were prompted to encapsulate the PPy nanoparticles with poly(methyl methacry-

[*] Prof. J. Jang, Dr. J. H. Oh
Hyperstructured Organic Materials Research Center and School of Chemical Engineering, Seoul National University
Shinlimdong 56-1, Seoul 151-742 (South Korea)
E-mail: jsjang@plaza.snu.ac.kr

[**] This work was financially supported by the Brain Korea 21 (BK 21) program of the Korean Ministry of Education, and by the Hyperstructured Organic Materials Research Center (HOMRC) supported by the Korean Science and Engineering Foundation (KOSEF).

  DOI: 10.1002/adfm.200400095

ADVANCED FUNCTIONAL MATERIALS

late) (PMMA), which is a typical transparent amorphous polymer used in glass substitutes. In order to minimize the loss of electrical conductivity, the coating thickness of PMMA was kept within nanometer dimensions.

Herein we report the fabrication, by two-step microemulsion polymerization, of PPy/PMMA core/shell nanospheres with tunable sizes of the core and shell parts. When the PPy/PMMA core/shell nanospheres were mixed with a PMMA matrix, the polymer nanocomposite film showed an excellent transparent conductive performance. The PMMA shell significantly reduces the aggregation of PPy nanoparticles and enhances the transmission of visible light. Furthermore, the nanometer-sized PMMA shell has a glass-transition temperature (T_g) lower than that of bulk PMMA. The PPy nanoparticles could be effectively linked by annealing the film at temperatures above T_g, and local electronic paths were generated without losing the high transparency. Coating the surface of the conducting-polymer nanoparticles conferred much greater stability under ambient conditions to the conductivity of the nanofillers by substantially reducing their oxidation. In addition, this polymer nanocomposite composed entirely of organic materials can be applied for the synthesis of highly transparent conductive films.

2. Results and Discussion

PPy/PMMA core/shell nanospheres were synthesized in a stepwise manner via microemulsion polymerization. The overall experimental procedure for the fabrication of PPy/PMMA core/shell nanospheres is illustrated in Scheme 1. Cationic surfactants such as dodecyltrimethylammonium bromide (DTAB), myristyltrimethylammonium bromide (MTAB), and cetyltrimethylammonium bromide (CTAB) were used to form micelles as nanoreactors. The pyrrole monomer was introduced into the micelle at room temperature (RT) and the chemical oxidation polymerization proceeded upon addition of ferric chloride. After the polymerization of the PPy core, the MMA monomer was subsequently introduced into the PPy-containing micelle at room temperature and polymerized at 70 °C by adding a water-soluble radical initiator.

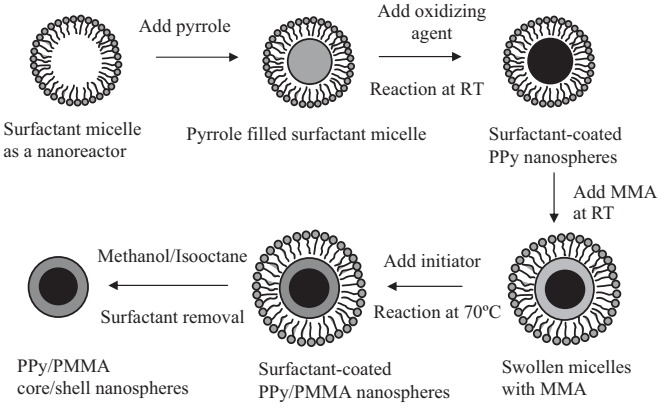

Scheme 1. Schematic diagram of the fabrication of PPy/PMMA core/shell nanospheres.

Figure 1a shows a scanning electron microscopy (SEM) image of PPy nanoparticles synthesized in 0.21 M aqueous DTAB solution. The PPy nanoparticles are composed entirely of spherical nanoparticles with an average diameter of 25 nm.

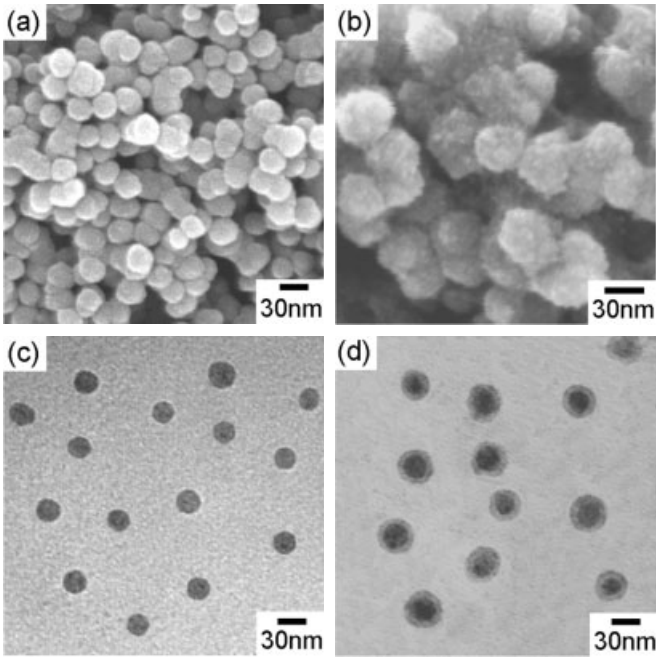

Figure 1. SEM and TEM images of PPy nanoparticles and PPy/PMMA core/shell nanospheres synthesized using a feed ratio of pyrrole/MMA of 1:2.5 (by wt.-%) in 0.21 M DTAB: a,b) SEM images; c,d) TEM images.

This means that the cationic surfactant micelles have acted successfully as nanoreactors for the synthesis of polymeric nanoparticles. Figure 1b shows the SEM image of PMMA-coated PPy nanospheres prepared with a pyrrole/MMA feed ratio of 1:2.5 (wt.-%) in 0.21 M DTAB. The PPy/PMMA core/shell nanospheres have an average diameter of 39 nm. It is likely that the micelles are swollen upon adding MMA in the second polymerization step. The transmission electron microscopy (TEM) image of pristine PPy nanoparticles (Fig. 1c) shows good agreement in the particle size with that of the SEM photograph. Figure 1d clearly exhibits the core/shell spherical structure of the PPy/PMMA nanocomposites. The average thickness of the PMMA shell is about 7 nm, which is also commensurate with the value obtained from the SEM data.

According to the SEM images, the PMMA shell has a raspberry structure. This is similar to the results obtained by Li et al.,[8,9] who synthesized PPy/polyacrylate core/shell particles by the heterocoagulation of large cationic PPy particles with small anionic polyacrylate beads followed by heat processing of the heterocoagulate units. The raspberry structure of the composite particles is considered to originate from the poor compatibility of PPy and PMMA.[8] Figure 2 shows high-resolution SEM images of PMMA-coated PPy nanoparticles synthesized at different feed ratios of monomers. Judging from these results, the raspberry structure is more apparent with decreas-

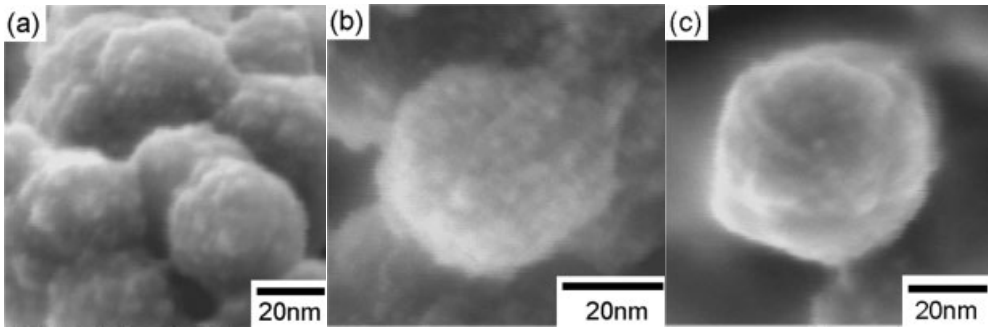

Figure 2. SEM images of PMMA-coated PPy nanoparticles synthesized using a feed ratio of pyrrole/MMA of: a) 1:1.25, b) 1:2.50, and c) 1:3.75 (by wt.-%) in 0.21 M DTAB.

ing PMMA shell thickness. As the thickness of PMMA shell decreases, the micro-phase separation of PMMA chains on the surface of PPy core occurs more easily, as they feel more interfacial tension; the mobility of PMMA chains is also enhanced in a thinner shell. At a large loading of MMA (Fig. 2c), the surface of the core/shell nanoparticles becomes smooth.

An energy-dispersive X-ray (EDX) analysis using a nanoprobe (ca. 4 nm) in scanning transmission electron microscopy (STEM) mode provided the composition of the core and shell parts directly. Figure 3a displays the EDX spectra of the shell moiety in the composite nanoparticle. It consists of C (64.9 %) and O (35.1 %) only. Since the MMA monomer has five C and two O atoms, the C/O weight ratio of PMMA is approximately 1.88. The C/O ratio (1.85) of the shell part is therefore very similar to that of pure PMMA. The composition obtained from core and shell parts was C (60.7 %), N (10.0 %), O (14.6 %), Fe (5.1 %), and Cl (9.6 %) (Fig. 3b). The Fe and Cl peaks originate from the doped iron-complex anion of the core PPy nanoparticle. Since a pyrrole has one N and four C atoms, the C/N weight ratio of PPy is about 3.43. This means that approximately 34.3 % C comes from the PPy core and 26.4 % from the PMMA shell. The estimated C/O ratio of the shell components is about 1.81, which is also similar to that of pure PMMA.

A Fourier-transform infrared (FT-IR) spectroscopic analysis also supported the observation that the synthesized polymer core/shell nanosphere consists of PPy and PMMA. Figure 4a shows the FT-IR spectrum of PPy nanoparticles. The FT-IR spectral baseline of conducting materials has a tendency to tilt owing to the plasma-reflection phenomenon.[10] The slanted baselines of PPy and the composite nanoparticles were therefore corrected with a multiple-point level. In the FT-IR spectrum of PPy, the peak at 1549 cm^{-1} is due to five-membered ring stretching and free C–N stretching vibrations. The band at 1485 cm^{-1} is attributed to the conjugated C–N stretching vibration. The characteristic FT-IR peaks of PMMA appear at 1731 and 1150 cm^{-1}, which are due to the C=O stretching and C–O stretching vibrations, respectively (Fig. 4b). The FT-IR band

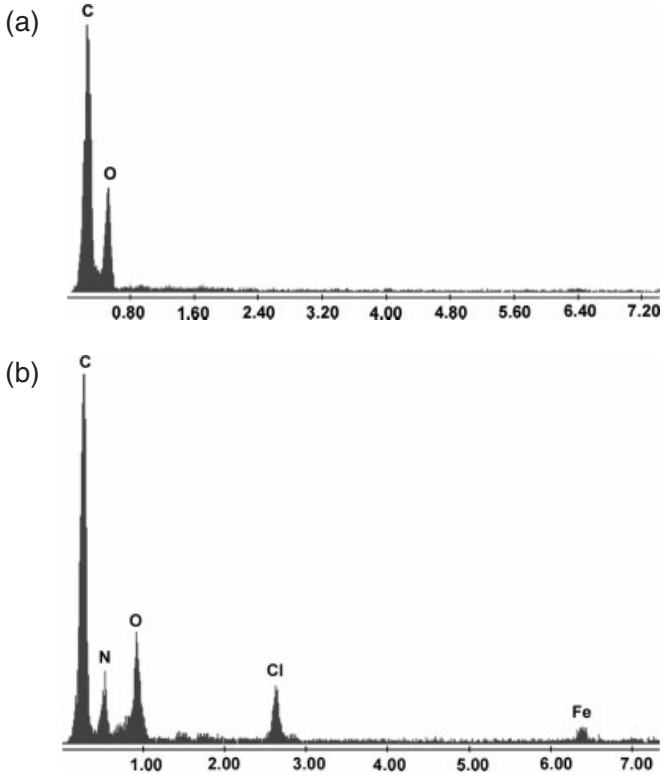

Figure 3. EDX spectra of PPy/PMMA core/shell nanospheres prepared using a feed ratio of pyrrole/MMA of 1:2.5 (by wt.-%) in 0.21 M DTAB: a) shell part and b) core and shell parts.

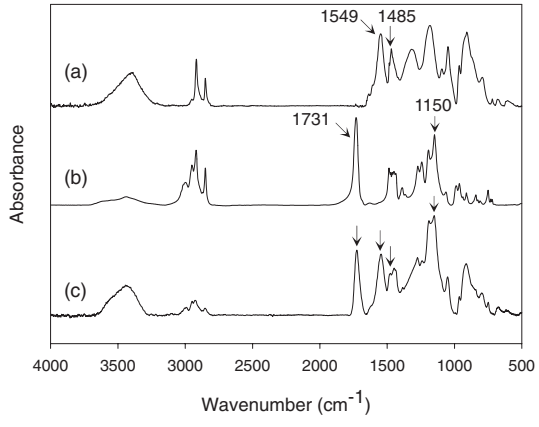

Figure 4. FT-IR spectra of: a) PPy, b) PMMA, and c) PPy/PMMA core/shell nanospheres synthesized using a feed ratio of pyrrole/MMA of 1:2.5 (by wt.-%) in 0.21 M DTAB.

ADVANCED FUNCTIONAL MATERIALS

assignments of PMMA and PPy are listed in Tables 1,2, respectively. Figure 4c shows the FT-IR spectrum of PPy/PMMA core/shell nanospheres synthesized using a pyrrole/MMA feed ratio of 1:2.5. The characteristic peaks of both PPy and PMMA appear in that spectrum.

Table 1. FT-IR peak assignment of PMMA.

Frequency [cm^{-1}]	Assignment
751	Skeletal + CH_2 rock
841, 964	Skeletal
988	C–O–C stretch
1150, 1195	C–O stretch
1241, 1277	C–O stretch
1387	CH_3 symmetric (umbrella) deformation
1448	CH_2 symmetric (scissors) deformation, O–CH_3 deformation
1485	CH_3 (α-methyl) asymmetric deformation
1731	C=O stretch
2850	Overtone of ester CH_3 deformation
2950	CH_3 (ester methyl) stretch
2998	CH_3 (α-methyl) stretch

Table 2. FT-IR peak assignment of PPy.

Wavenumber [cm^{-1}]	Assignment
783	C–H wag
1549	Ring stretch band
	Free C–N stretch
1485	Conjugated C–N stretch
2851, 2925	C–H stretch
3403	N–H stretch

Figure 5 shows the carbonyl-peak shift upon increasing the PPy content in the PPy/PMMA core/shell nanoparticles. As the composition of PPy in the composite nanoparticle increases, the carbonyl band of PMMA appears as broader peak at lower wavenumber (1724 cm^{-1}). This is due to hydrogen bonding between the N–H groups of PPy and the C=O groups of PMMA that is facilitated upon increasing the PPy content. In other words, the red-shift originates from the fact that a greater portion of carbonyl groups form hydrogen bonds at the interface between the PPy core and the PMMA shell in a thinner PMMA shell than in a thicker shell.

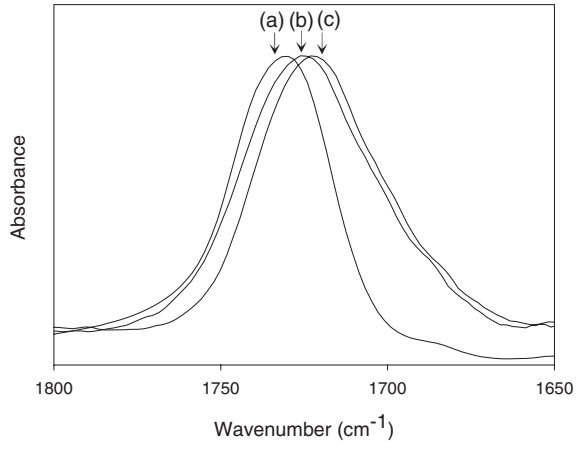

Figure 5. Carbonyl-peak shift in the FT-IR spectra of: a) pure PMMA, b) PPy/PMMA (1:3.75), and c) PPy/PMMA (1:2.50).

The variation in the average diameter of the PPy/PMMA core/shell nanoparticles as a function of surfactant concentration is illustrated in Figure 6a. Under our experimental conditions the average diameter of PPy/PMMA core/shell nanoparticles was tunable from about 25 nm to 84 nm by controlling the surfactant concentration and the surfactant alkyl-chain length. As the surfactant amount increases, the PPy/PMMA nanoparticle size decreases. The micelle aggregation number (n), which is the number of surfactant molecules required to form a micelle, is independent of the surfactant concentration to fairly high surfactant concentrations.[11] Therefore, the number of micelles increases with increasing surfactant concentration, which induces a size reduction of the nanoparticles at a fixed monomer amount. On the other hand, the nanoparticle size increases with increasing surfactant chain-length. The value of n becomes smaller with shorter chain length.[11] Thus, the number of micelles increases with shorter spacer length at the same surfactant concentration, which results in a reduction in the particle size. In addition, the flexibility of the surfactant alkyl chain is facilitated in a longer spacer. The enhanced flexibility of the longer spacer provides more free volume inside the micelle as a monomer reservoir. This phenomenon leads to the production of larger particles in surfactant micelles with longer spacers.

The size of the core and shell parts could easily be controlled by changing the feeding amount of monomers. Figure 6b reflects the average diameter change of PPy nanoparticles upon increasing the feeding amount of pyrrole. The micelles were formed using 0.23 M of CTAB. The diameter of PPy nanoparticles increases in proportion to the input amount of the monomer. This arises from the fact that the size of the micelle increases to some degree upon increasing the feeding amount of monomers.[12] Figure 6c exhibits the variation in the average shell thickness as a function of the input amount of MMA. For the synthesis of the core moiety, 1.0 g of pyrrole was added to the micellar solution of 0.23 M CTAB. The average PMMA shell thickness increases gradually from about 5.6 nm to 13.5 nm upon increasing the feeding amount of MMA from 1.25 g to 5.0 g.

Figures 7a,b indicate the transparencies of PPy/PMMA composite films with conductive-filler contents of 10 wt.-% and 20 wt.-%, respectively, compared with that of pure PMMA. In order to investigate the effect of the conductive filler size and shape on the transparencies of composite films, PMMA-coated PPy nanoparticles (PPy/PMMA = 1:2.5 by wt.-%), uncoated PPy nanoparticles, and bulk PPy particles were employed as the conductive filler. As described before, the PMMA-coated PPy nanoparticles consisted of a PPy core with an average diameter of 25 nm and a PMMA shell with a thickness of about 7 nm. The uncoated PPy nanoparticles also had an average diameter of 25 nm. The bulk PPy particles were synthesized by

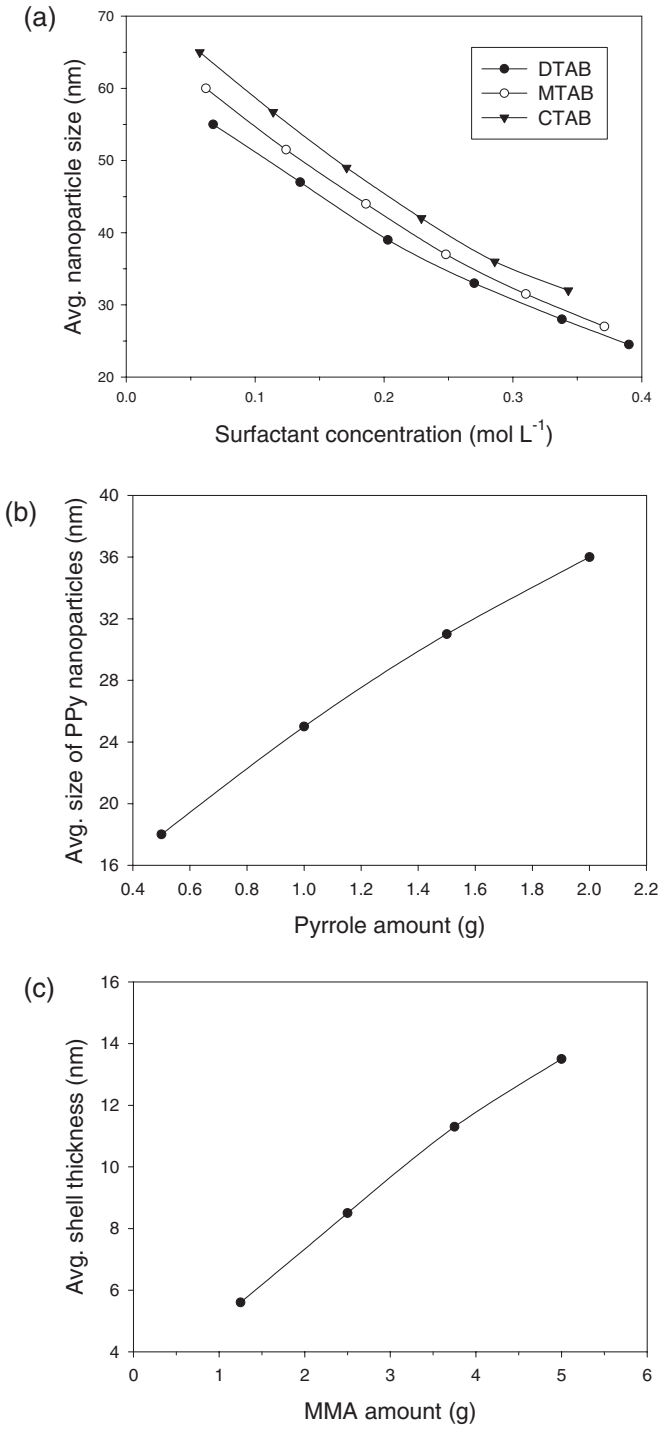

Figure 6. a) Average-diameter changes of PPy/ PMMA core/shell nanoparticles as a function of surfactant concentration. b) Average-diameter variations of PPy core as a function of pyrrole feeding amount. c) Average-shell-thickness changes of PMMA shell as a function of MMA feeding amount.

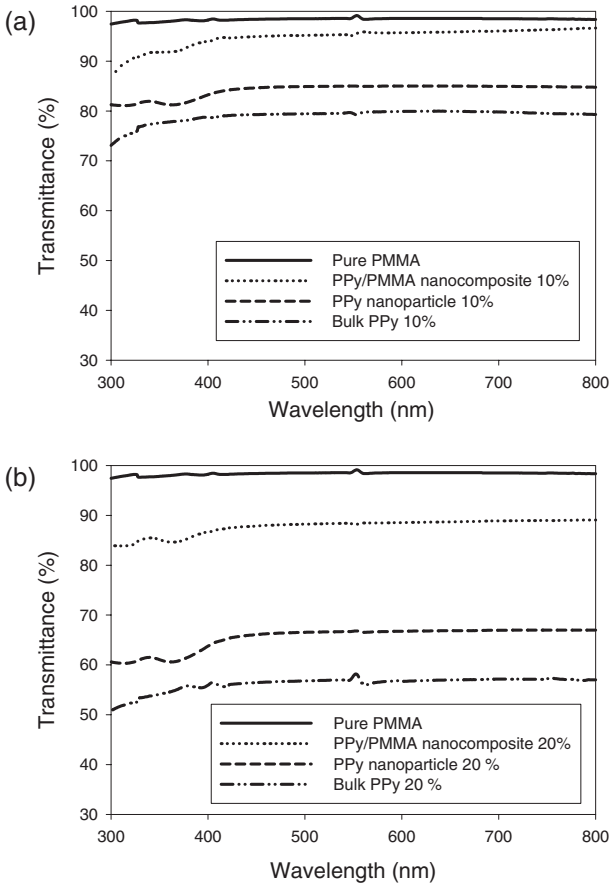

Figure 7. Optical transparency of composite films with a conductive-filler content of: a) 10 wt.-% and b) 20 wt.-%.

dispersion polymerization without surfactants and had a broad size distribution of 100–200 nm diameter. The PPy/PMMA composite thin films were prepared by compression molding under 4000 psi (2.76×10^7 Pa) at 200 °C for 10 min. The polymer film thickness was adjusted to about 20 μm by using a polyimide spacer and controlling the feeding amount of powders.

The polymer-composite film containing PMMA-coated PPy nanoparticles shows an enhanced transparency (up to 30 %) compared with those of films containing uncoated PPy fillers. At a filler content of 10 wt.-%, the PMMA-coated PPy nanoparticles/PMMA film shows an excellent optical transmission, above 90 % in the whole visible-light region. When the conductive-filler content was increased to 20 wt.-%, the PMMA-coated PPy nanoparticles/PMMA film still exhibit a high optical transmission, above 83 % in the whole visible-light region. However, the uncoated PPy nanoparticle/PMMA films have poor transmission (below 65 %), and the dispersion-polymerized PPy/PMMA film has a still worse transmission (below 55 %). The PMMA shell, which is identical to the matrix polymer, promotes the compatibility and dispersion of the conductive nanofiller and improves the optical transmissions of the composite films.

Figure 8 reveals the variation in the electrical conductivity of composite films as a function of PPy content. The percolation threshold of PPy nanoparticles and bulk PPy particles (showing an abrupt rise in the electrical conductivity of approximately three orders of magnitude) was observed in the range between

ADVANCED FUNCTIONAL MATERIALS

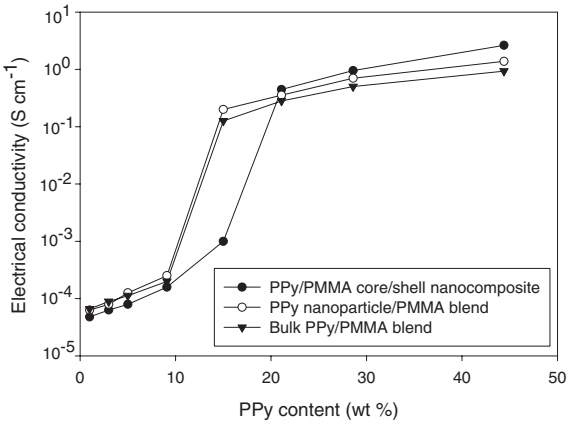

Figure 8. Electrical-conductivity change of composite films upon increasing the PPy content.

10 wt.-% and 15 wt.-%. In contrast, the percolation threshold of PMMA-coated PPy nanofillers occurred on changing from 15 wt.-% to 20 wt.-%. It is noteworthy to consider that the typical conductivity of chemically synthesized PPy lies in the range of 10^0 to 10^1 S cm^{-1}. The percolation threshold is a function of the dimensionality of the system, and of the shape (more specifically the aspect ratio ($a = L/w$), where L = length and w = width) of the active fillers that give rise to the mentioned phenomenon.[13] In this experiment, the generation of local electronic paths to reach the bulk conductivity of PPy is retarded by 5 wt.-% of PPy/PMMA core/shell nanospheres in the polymer nanocomposites because of the insulating PMMA shell. However, beyond this threshold, the conductivity of the PMMA-coated PPy nanofillers/PMMA film is higher than those of uncoated PPy fillers. This is due to the well-dispersed conductive fillers. At a high composition of conductive fillers above the percolation threshold, uncoated PPys are more aggregated on a larger scale than with PMMA-coated PPy nanoparticles. However, as mentioned before, a PMMA shell identical with the matrix polymer enhances the compatibility of the nanofillers with the matrix and facilitates the effective dispersion of the PPy/PMMA core/shell nanofillers. This phenomenon creates more electronic paths in a larger dimension expanding over all areas of the polymer-composite films at a high conductive-filler content.

In order to improve the electrical conductivity of the polymer film, the PPy was doped with a small amount of iodine during the microemulsion polymerization. According to a UV-Vis spectroscopic investigation, undoped PPy nanoparticles have a band-gap energy (E_g) of 3.17 eV. The doped PPy nanoparticles show a lower E_g of 2.86 eV. The electrical conductivity of doped PPy nanoparticles is 237 S cm^{-1}, which is a value two orders of magnitude higher than that of undoped PPy nanoparticles. The polymer-composite film containing the PMMA-coated doped PPy nanoparticles of 20 wt.-% exhibits a high electrical conductivity of 116 S cm^{-1}, together with a high optical transparency (ca. 81 %). In addition, while the electrical conductivity of uncoated PPy fillers decreased by a magnitude of 10^2–10^3 over a month, that of PMMA-coated PPy nanofillers was reduced by only 10^0–10^1 magnitude over the same time period. The coating of the surface of PPy nanoparticles confers a higher stability of electrical conductivity under ambient conditions by reducing the degree of oxidation.

The insulating PMMA shell seems to hamper the formation of a network of the conducting fillers up to a fairly high filler content. However, the formation of conductive-filler networks was not severely hindered under our experimental conditions. A differential scanning calorimetry (DSC) analysis provided the answer to the formation of the conductive-filler networks at a relatively low filler content. Figure 9 presents the T_g variations of PMMA as a function of PMMA content in the PPy/PMMA core/shell nanospheres. The T_g of PMMA is reduced upon decreasing PMMA content, i.e., with a thinner PMMA shell. The T_g of pure PMMA is 105.1 °C. However, when the core/shell nanospheres contain 55.6 % PMMA, the T_g of

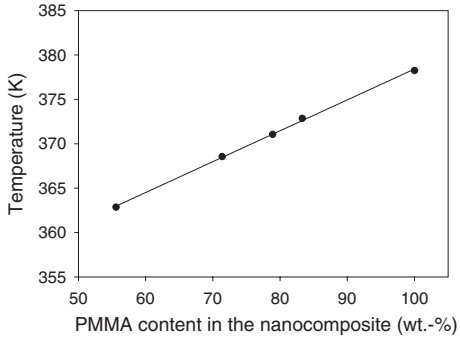

Figure 9. Glass-transition temperature (T_g) as a function of PMMA content in the nanocomposite.

PMMA is only about 89.7 °C. According to the degree of interaction between the polymer chain and the solid substrate, the T_g at the interface region can be different from the bulk value. An increase of T_g with decreasing film thickness has been found for other polymers for which the interaction is known to be strongly attractive.[14] In contrast, it has been reported that for the combination of a polymer and substrate that have no specific interaction, the influence on T_g of the substrate is trivial and this sample shows only a decrease of T_g with decreasing film thickness.[15] In our experiment, the reduction of T_g with decreasing shell thickness reveals that the two polymers possess poor compatibility as a whole. Even though hydrogen bonding between the carbonyl group of PMMA and the N–H group could occur at the interface, this interaction is not intense enough to prevent the relaxation behavior of the polymer chains. The conductive polymer thin films were prepared by high-temperature compression molding. During the fabrication process of the polymer-composite film, the conductive-filler networks could be formed through additional annealing effects at temperatures (200 °C) above T_g.

Figure 10 shows a schematic representation of the film prepared using different conductive fillers (PMMA-coated PPy nanoparticles and uncoated PPy nanoparticles) at a filler content above the percolation threshold. During the manufacturing

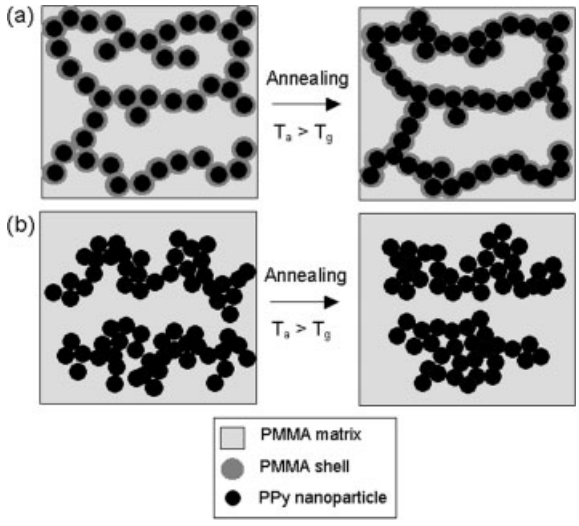

Figure 10. Schematic illustration of the formation of conductive-filler networks in the polymer-composite film prepared using different conductive fillers: a) PMMA-coated PPy nanoparticles and b) uncoated PPy nanoparticles. The filler content was above the percolation threshold. T_a is the annealing temperature.

process of the thin films, heat treatment above the T_g of the PMMA shell exerts an annealing effect on the conductive fillers. The PMMA-coated PPy nanoparticles could be brought into contact by the pressure of compression molding (4000 psi) and the annealing effect of the film. The annealing effect is considered to stem from the poor compatibility between PMMA and PPy. However, during the annealing process, uncoated PPy nanoparticles are prone to be relatively more aggregated because of the phase separation. The slightly higher electrical conductivity of the PMMA-coated PPy nanofiller/PMMA film at a high filler content than those of uncoated PPy fillers is presumably due to this phenomenon—more electronic paths are generated in a larger dimension expanding over all the area of the film for the PMMA-coated PPy nanofiller/PMMA film.

It is possible that the raspberry structure of the thin PMMA shell helps the electrical current flow. In addition, the presence of partially coated PPy nanoparticles, even though the content of them (less than 10 %) is not so high, is believed to also be beneficial to the current flow. However, the important point is that the core/shell nanoparticles without a raspberry structure, and partially coated PPy nanoparticles, which were synthesized by using a large amount of MMA, show a percolation threshold in the polymer-composite film. The core/shell nanoparticles synthesized using a feed ratio of pyrrole/MMA of 1:3.75 (the SEM image is shown in Fig. 2c) also show a percolation threshold on going from 25 wt.-% to 30 wt.-%. This confirms that the pressure-assisted annealing effect in the manufacturing process of the films plays the most important role in the current flow. Doping of iodine facilitates the effective formation of polarons and bipolarons in the PPy chains and promotes the flow of electrical current through the conductive-filler networks.

Figure 11 presents SEM images of the fractured surface of PPy/PMMA composite films. The SEM images of the composite films containing PMMA-coated PPy nanoparticles display the formation of conductive-filler networks (marked as arrows

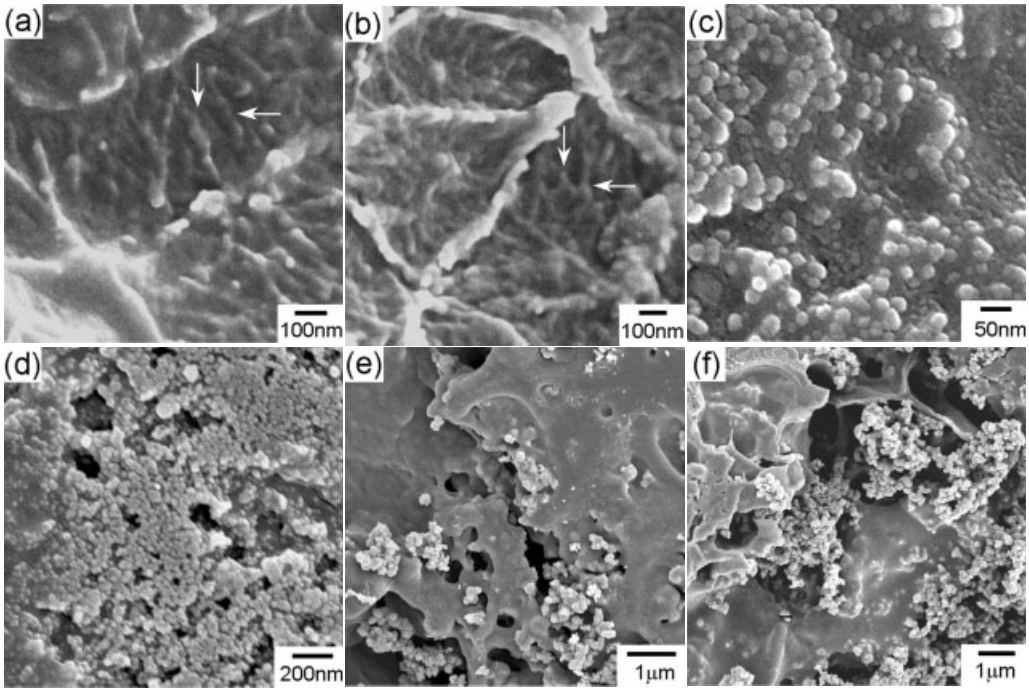

Figure 11. SEM images of the fractured surface of composite films: a) PPy/PMMA core/shell nanoparticle (10 wt.-%), b) PPy/PMMA core/shell nanoparticle (20 wt.-%), c) PPy nanoparticles (10 wt.-%), d) PPy nanoparticles (20 wt.-%), e) bulk PPy particles (10 wt.-%), and f) bulk PPy particles (20 wt.-%). The arrows indicate the network of conductive nanofillers.

ADVANCED FUNCTIONAL MATERIALS

in Figs. 11a,b) and demonstrate the good dispersion of the networks in the PMMA matrix. The conductive-filler network shows the morphology of a noded fibril, which provides evidence for the presence of the annealing of the PMMA shells. The formation of conductive-filler networks is promoted upon increasing the filler content, but without large-scale aggregation. In contrast, the dispersion of uncoated PPy fillers is worse than that of PMMA-coated PPy nanofillers. The uncoated PPy nanoparticles with similar dimensions to those of composite nanofillers exhibit an intermediate level of dispersion between that of the PMMA-coated PPy nanoparticle/PMMA film and the bulk PPy nanoparticle/PMMA film (Figs. 11c,d). The fractured surfaces of bulk PPy particle/PMMA films exhibit large-scale aggregation in the PMMA matrix (Figs. 11e,f); the aggregation becomes severe upon increasing the filler content. These agglomerates seem to cause the rapid deterioration in the optical transparency at a high filler content. The SEM analysis substantiates the fact that the dispersion of conductive fillers is favored for fillers with a smaller size and greater compatibility with the polymer matrix.

To evaluate the thermal stability of the PPy/PMMA core/shell nanospheres, thermogravimetric analysis (TGA) was performed. Figure 12 demonstrates the TGA thermogram of the PMMA-coated PPy nanoparticles. A drastic weight loss of the composite particles was observed in the temperature range

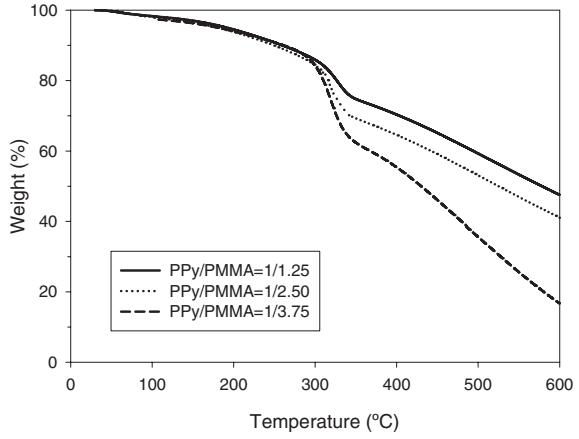

Figure 12. TGA thermograms of PPy/PMMA core/shell nanospheres.

300–400 °C and the thermal degradation of PPy/PMMA core/shell nanospheres increased with increasing PMMA content. It can be considered that the thermal degradation of the PMMA shell mainly occurs in this temperature range. It has been reported previously that loss of nitrogen occurs between 400 and 600 °C and polycondensed graphitic species are generated during the carbonization process of a doped PPy.[16]

3. Conclusions

PPy/PMMA core/shell nanospheres with an average diameter of several tens of nanometers were synthesized via a two-step microemulsion polymerization procedure. The size of the core and shell parts was easily controlled by changing the amount of surfactant and of monomer feed. When PMMA-coated PPy nanoparticles (10 wt.-%) were compression-molded with PMMA matrix at a high temperature above T_g, the nanocomposite thin films showed an excellent optical transparency, above 90 % in the whole visible-light range. As the content of the core/shell nanofillers increased to 20 wt.-%, the nanocomposite films still exhibited a high optical transmission, above 83 % in the whole visible-light region. The transparency of the film containing PPy/PMMA core/shell nanoparticles is higher (up to 30 %) than those of films containing uncoated PPy nanoparticles with similar dimensions and bulk PPy particles with diameters of several hundreds of nanometers. On the other hand, the percolation threshold in the electrical conductivity of the films containing composite nanoparticles was observed at a filler content of between 15 and 20 wt.-%, which is higher by 5 wt.-% owing to the insulating PMMA shell. Above the percolation threshold, the PMMA-coated PPy nanoparticles show an enhanced conductivity due to the formation of conductive-filler networks and good dispersion of the networks. The efficient formation of the conductive-filler networks is related to the annealing effect of the thin PMMA shell. The PMMA shell also promotes the compatibility of the conductive fillers with the polymer matrix and promotes good dispersion of the PPy nanofillers. The electrical conductivity of the polymer-composite film could be enhanced by two orders of magnitude by doping the PPy core with iodine. The synthesized PPy/PMMA core/shell nanospheres could be successfully utilized as an effective conductive filler for the preparation of a highly transparent conductive thin film. In addition, the highly transparent conductive films composed entirely of organic materials have good flexibility, which might provide a promising advantage for practical applications.

4. Experimental

Materials: Pyrrole, iron(III) chloride, methanol, and 2,2,4-trimethylpentane were obtained from Aldrich and used as received. Methyl methacrylate was received from Junsei Chemical Co. and purified with an inhibitor-removing column. 2,2′-Azobis(2-methylpropionamidine) dihydrochloride (AMPAD) was purchased from Aldrich and used as an initiator. DTAB, MTAB, and CTAB were purchased from Fluka and used as received.

Synthesis of Conductive Fillers: A variable amount of cationic surfactant was magnetically stirred in 40 mL of distilled water at room temperature. In a typical synthesis of PPy/PMMA core/shell nanospheres, 1.0 g (14.9 mmol) of pyrrole was added dropwise to the surfactant solution, and 5.56 g (34.3 mmol) of iron(III) chloride dissolved in 5 mL of distilled water was added to the surfactant/pyrrole solution. For the doping of PPy, 454 mg (3.58 mmol) of iodine was added to the micellar solution. The chemical oxidation polymerization of PPy in micelles proceeded with magnetic stirring for 3 h at room temperature. A different amount of MMA (1.25, 2.50, 3.75, or 5.00 g) was then added dropwise to the reaction vessel at room temperature, and the flask was placed in a water bath previously heated to 70 °C. AMPAD (1.5 wt.-% based on the amount of MMA) dissolved in 3 mL of distilled water was added to the reaction vessel. The microemulsion polymerization of PMMA proceeded for 2 h at 70 °C. The reaction product was then placed in a separating funnel and excess methanol was added to remove the surfactants and the residual iron(III) chloride. The precipita-

tion of the PPy nanoparticles was promoted by adding a small amount of isooctane owing to the enhanced hydrophobicity. The upper solution containing surfactants was discarded and the nanocomposite precipitate was dried in a vacuum oven at room temperature. The uncoated PPy nanoparticles were prepared by quenching the polymerization of PPy by adding excess methanol. Bulk PPy particles were fabricated by dispersion polymerization without using surfactants.

Preparation of Polymer-Composite Thin Films: A variable amount of the nanofillers—PPy/PMMA core/shell nanoparticles, uncoated PPy nanoparticles, and bulk PPy particles—was mixed with PMMA powder. The PPy/PMMA composite thin films were prepared by compression molding under 4000 psi at 200 °C for 10 min. The polymer-film thickness was adjusted to about 20 μm by using a polyimide spacer and controlling the feeding amount of the powders.

Instrumental Analysis: TEM images were taken with a JEOL 2000FX analytical microscope operating at an accelerating voltage of 200 kV. SEM images were obtained using a JEOL 6330F microscope operating at 5 kV. EDX analysis was carried out with a Philips CM-20 microscope coupled with an EDX facility. FT-IR spectra were recorded on a Bomem MB 100 FT-IR spectrometer equipped with a deuterated triglycine sulfate (DTGS) detector. FT-IR spectra were obtained over 32 scans in absorption mode at a resolution of 4 cm^{-1}. The UV-vis spectra were recorded with a Perkin-Elmer Lambda-20 spectrometer. The electrical conductivity was determined by the four-probe method using a Keithley 2400 instrument. DSC analysis was performed with a TA DSC-2010 at a heating rate of 10 °C min^{-1}. TGA thermograms were obtained with a TA Q-500 thermogravimetric analyzer.

Received: March 5, 2004
Final version: June 23, 2004

[1] a) J. Cui, A. Wang, N. L. Edleman, J. Ni, P. Lee, N. R. Armstrong, T. J. Marks, *Adv. Mater.* **2001**, *13*, 1476. b) M. Mas-Torrent, E. Laukhina, C. Rovira, J. Veciana, V. Tkacheva, L. Zorina, S. Khasanov, *Adv. Funct. Mater.* **2001**, *11*, 299. c) M. Miyakawa, K. Hayashi, M. Hirano, Y. Toda, T. Kamiya, H. Hosono, *Adv. Mater.* **2003**, *15*, 1100. d) H. Ohta, T. Kambayash, M. Hirano, H. Hoshi, K. Ishikawa, H. Takezoe, H. Hosono, *Adv. Mater.* **2003**, *15*, 1258. e) M. P. Taylor, D. W. Readey, C. W. Teplin, M. F. A. M. van Hest, J. L. Alleman, M. S. Dabney, L. M. Gedvilas, B. M. Keyes, B. To, P. A. Parilla, J. D. Perkins, D. S. Ginley, *Macromol. Rapid Commun.* **2004**, *25*, 344. f) W. S. Seo, H. H. Jo, K. Lee, J. T. Park, *Adv. Mater.* **2003**, *15*, 795.

[2] a) D. B. Cairns, M. A. Khan, C. Perruchot, A. Riede, S. P. Armes, *Chem. Mater.* **2003**, *15*, 233. b) S. F. Lascelles, S. P. Armes, *J. Mater. Chem.* **1997**, *7*, 1339. c) M. Omastová, J. Pavlinec, J. Pionteck, F. Simon, S. Košina, *Polymer* **1998**, *39*, 6559. d) J. Jang, B. Lim, J. Lee, T. Hyeon, *Chem. Commun.* **2001**, 83.

[3] a) Y. Cao, G. M. Treacy, P. Smith, A. J. Heeger, *Synth. Met.* **1993**, *57*, 3526. b) J. J. Apperloo, J. A. E. H. van Haare, R. A. J. Janssen, *Synth. Met.* **1999**, *101*, 417.

[4] a) F. M. Huijs, F. F. Vercauteren, G. Hadziioannou, *Synth. Met.* **2002**, *125*, 395. b) F. M. Huijs, F. F. Vercauteren, B. de Ruiter, D. Kalicharan, G. Hadziioannou, *Synth. Met.* **1999**, *102*, 1151, c) F. M. Huijs, J. Lang, D. Kalicharan, F. F. Vercauteren, J. J. L. van der Want, G. Hadziioannou, *J. Appl. Polym. Sci.* **2001**, *79*, 900.

[5] D. Shibuta, *US Patent 5 853 877*, **1996**.

[6] a) A. Tracz, J. K. Jeszka, A. Sroczynska, M. Kryszewski, S. Schrader, K. Pfeiffer, J. Ulanski, *Adv. Mater. Opt. Electron.* **1996**, *6*, 330. b) A. Tracz, J. K. Jeszka, A. Sroczynska, J. Ulanski, J. Plocharski, H. Yamochi, S. Horiuchi, G. Saito, *Synth. Met.* **1997**, *86*, 2173.

[7] J. Jang, J. H. Oh, G. D. Stucky, *Angew. Chem. Int. Ed.* **2002**, *41*, 4016.

[8] H. Li, J. Han, A. Panioukhine, E. Kumacheva, *J. Colloid Interface Sci.* **2002**, *255*, 119.

[9] H. Li, E. Kumacheva, *Colloid Polym. Sci.* **2003**, *281*, 1.

[10] H. S. Nalwa, *Handbook of Organic Conductive Molecules and Polymers*, Vol. 4, 1st ed., Wiley-VCH, Chichester, UK **1997**, Ch. 9.

[11] a) J. Jang, J. H. Oh, *Chem. Commun.* **2002**, 2200. b) J. Jang, J. H. Oh, *Adv. Mater.* **2003**, *15*, 977.

[12] a) J. Jang, H. Ha, *Langmuir* **2002**, *18*, 5613. b) J. Jang, H. Ha, *Chem. Mater.* **2003**, *15*, 2109.

[13] G. Torres-Delgado, C. I. Zúñiga-Romero, O. Jiménez-Sandoval, R. Castanedo-Pérez, B. Chao, S. Jiménez-Sandoval, *Adv. Funct. Mater.* **2002**, *12*, 129.

[14] a) J. L. Keddie, R. A. L. Jones, R. A. Cory, *Faraday Discuss.* **1994**, *98*, 219. b) J. H. Van Zanten, W. E. Wallace, W. Wu, *Phys. Rev. E* **1996**, *53*, R2053.

[15] a) J. L. Keddie, R. A. L. Jones, R. A. Cory, *Europhys. Lett.* **1994**, *27*, 59. b) W. E. Wallace, J. H. van Zanten, W. Wu, *Phys. Rev. E* **1995**, *52*, R3329. c) J. H. Kim, J. Jang, W. C. Zin, *Langmuir* **2001**, *17*, 2703.

[16] E. Ando, S. Onodera, M. Iino, O. Ito, *Carbon* **2001**, *39*, 101.

